Target engagement studies and kinetic live-cell degradation assays enable the systematic characterization of HDAC6 PROTACs at endogenous protein expression levels

Maria Hanl,[1] Felix Feller,[1] Irina Honin,[1] Kathrin Tan,[1] Linda Schäker-Hübner,[1] Nico Bückreiß,[1] Matthias Schiedel,[2] Michael Gütschow,[3] Gerd Bendas,[1] and Finn K. Hansen[1]*

[1]Department of Pharmaceutical and Cell Biological Chemistry, Pharmaceutical Institute, University of Bonn, An der Immenburg 4, 53121 Bonn, Germany.

[2]Institute of Medicinal and Pharmaceutical Chemistry, Technische Universität Braunschweig, Beethovenstraße 55, 38106 Braunschweig, Germany.

[3]Department of Pharmaceutical and Medicinal Chemistry, Pharmaceutical Institute, University of Bonn, An der Immenburg 4, 53121 Bonn, Germany.

ABSTRACT

Histone deacetylase 6 (HDAC6) is an important drug target for the treatment of cancer, inflammation, and neurodegenerative disorders. In recent years, the development of proteolysis-targeting chimeras (PROTACs) has emerged to achieve the chemical knockdown of HDAC6. Consequently, there is an urgent need to develop efficient methods for target engagement studies and to enable a thorough characterization of the degradation efficiency and kinetics of HDAC6 PROTACs. In this work, we present a simple NanoBRET assay to assess HDAC6 cellular target engagement using a HeLa$^{HDAC6\text{-}HiBiT}$ cell line that stably expresses the LgBiT protein. For this purpose, we successfully designed, synthesized, characterized, and utilized the cell permeable TAMRA-based fluorescent ligand **5**. The key advantage of this NanoBRET assay using HeLa$^{HDAC6\text{-}HiBiT}$ cells is the endogenous HDAC6 expression, allowing us to study binding of inhibitors in a native environment. Furthermore, we succeeded in establishing a system for kinetic live cell monitoring of HDAC6 degradation. The analysis of the degradation kinetics of a set of HDAC6 PROTACs provided detailed insights into their degradation efficiency and will be helpful for the development of improved HDAC6 degraders in the future.

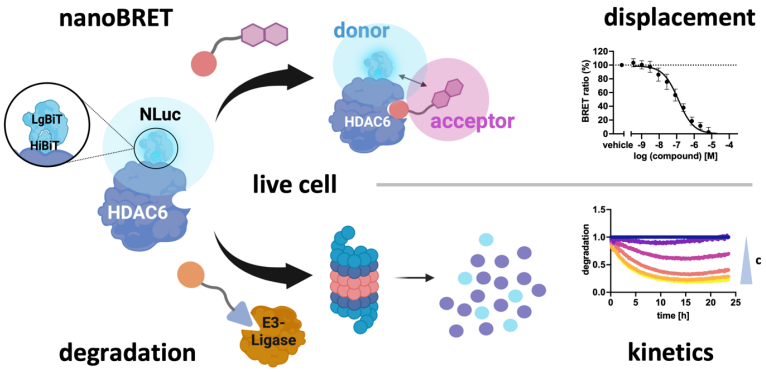

KEYWORDS

Degradation kinetics, HDAC6, NanoBRET, PROTAC, targeted protein degradation

INTRODUCTION

Protein acetylation regulates the cellular functions of proteins in the nucleus and cytoplasm and is modulated by histone acetyltransferases (HATs) and histone deacetylases (HDACs).[1] HDACs catalyze the deacetylation of ε-amino groups of lysine residues in both histone and non-histone proteins. 18 HDACs have been identified in humans and are classified into four classes based on their sequence homology: class I (HDAC1, HDAC2, HDAC3 and HDAC8), class II (IIa: HDAC4, HDAC5, HDAC7, and HDAC9, IIb: HDAC6 and HDAC10), class III (SIRT1, SIRT2, SIRT3, SIRT4, SIRT5, SIRT6, and SIRT7) and class IV (HDAC11). Class I, II, and IV are Zn^{2+}-dependent enzymes, while class III isoforms require NAD^+ as a cofactor.[2–4]

HDAC6 plays a unique role within the HDAC family. Due to its predominant cytoplasmic localization, HDAC6 exhibits distinct substrate specificity, targeting non-histone proteins such as Hsp90, α-tubulin, HSF-1, peroxiredoxin, and cortactin. HDAC6 is involved in numerous physiological cellular processes, such as protein trafficking, angiogenesis, inflammation, and cell migration.[5,6] Dysregulation of HDAC6 activity is associated with neurodegenerative diseases, various types of cancer, and pathological autoimmune responses.[7–11]

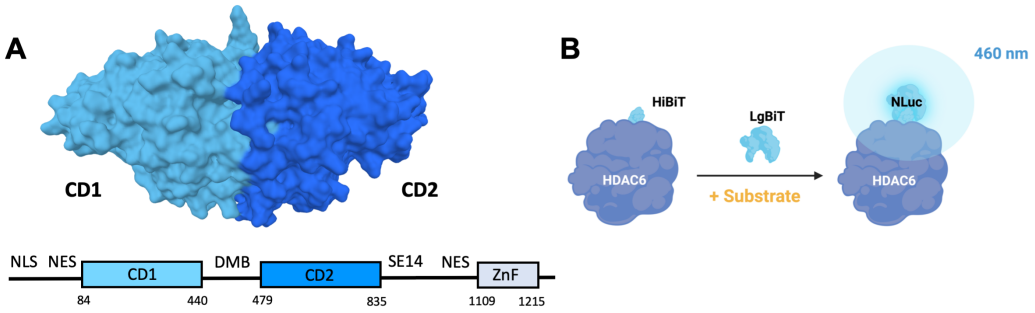

Figure 1. A: Illustration of HDAC6 (PDB: 7QNO, from *Danio rerio*). NLS: nuclear localization signal, NES: nuclear export signal, DMB: dynein motor binding, SE14: serine-glutamate

tetradecapeptide repeat, ZnF: ubiquitin-binding zinc finger binding domain, CD1: catalytic domain 1, CD2: catalytic domain 2. **B**: Schematic illustration of the HiBiT principle. The active NLuc is formed through binding of the LgBiT to the HiBiT subunit. After the addition of a substrate, a bioluminescence signal can be detected.

HDAC6 has unique structural characteristics, including two enzymatically active catalytic domains (CD1 and CD2) (Figure 1A). While the function of CD1 remains poorly understood, the CD2 is well characterized for its role in deacetylation.[12] A dynein motor binding domain (DMB) between these domains facilitates cargo transport along microtubules.[6] In addition, a ubiquitin-binding zinc finger domain (ZnF-UBP) at the C-terminus promotes the clearance of misfolded proteins.[9,13,14]

To date, five HDAC inhibitors (HDACi) with limited selectivity have been approved by the U.S. Food and Drug Administration (FDA) and the European Medicines Agency (EMA): vorinostat, belinostat, panobinostat, romidepsin, and givinostat. The combination of HDACi with other chemotherapeutic agents or targeted therapies has demonstrated potential as a therapeutic strategy in the treatment of cancer.[15,16] However, non-selective HDACi are frequently associated with severe adverse effects such as nausea, fatigue, and hematologic toxicities.[17–21] Thus, selective inhibitors are expected to result in fewer side effects. For instance, HDAC6-preferential inhibitors, such as ricolinostat or citarinostat, are currently in clinical trials, and more recently, highly selective HDAC6 inhibitors have entered clinical trials.[22]

HDAC6 activity can be inhibited either by HDAC6 inhibitors or by protein knockdown using the proteolysis-targeting chimera (PROTAC) technology.[23] Targeted protein degradation (TPD) *via* PROTACs is an emerging strategy for innovative drug discovery that may offer distinct advantages over classical occupancy-driven inhibitors.[8,24] Several compounds, e.g. vepdegestrant, bavdegalutamide, and CFT8634, have entered clinical trials in recent years.[25–27]

Classical drug design is based on well-defined active sites suitable for small molecules with appropriate pharmacological effects.[28] However, the design of efficient PROTACs is considerably more complex. PROTACs act through the ubiquitin-proteasome system (UPS), hijacking the intrinsic proteasomal pathway and resulting in a cellular target protein knockdown. PROTACs are typically designed as heterobifunctional molecules consisting of two ligands: one that targets the protein of interest (POI) and another that binds to an E3 ligase, connected by a suitable linker.[29,30] Protein degradation *via* PROTACs is a multistep, event-driven process coordinated by multiple factors. Once they have reached the target proteins, PROTACs must form binary complexes with the POI or the E3 ligase. These binary complexes facilitate the formation of a stable POI:PROTAC:E3 ligase ternary complex, which promotes polyubiquitination. Subsequently, the polyubiquitinated POI is recognized and degraded by the proteasome.[25,28,31] A key pharmacological advantage of PROTACs is that they facilitate degradation at sub-stoichiometric concentrations relative to the POI.[31] Binding affinity does not necessarily correlate with degradation potency; even PROTACs possessing ligands with low affinity can still exert efficient degradation.[23,32,33] Multiple factors influence the efficacy of PROTACs. For instance, high-affinity binary complexes with a PROTAC can lead to a hook effect at high concentrations, where unproductive binary complexes prevent ternary complex formation.[34] In contrast, low-affinity binary complexes can sometimes lead to strong degradation.[35] Moreover, the choice of linker length and flexibility also influences degradation outcomes.[28,34] It remains a challenge to predict which molecular features are responsible for the formation of a cooperative, stable ternary complex and efficient degradation.[36,37]

The design and optimization of PROTACs is often based on empirical data and extensive chemical optimization.[38] To better understand these processes in living cells while increasing the predictability of PROTAC activity, it is crucial to develop suitable assay systems. The study of drug-target engagement in living cells is an essential step in drug development.[39] Therefore, we

aimed to develop a NanoBRET assay to investigate the formation of HDAC6:PROTAC binary complexes in an endogenous cellular environment. Traditionally, cellular HDAC6 target engagement studies have relied on antibody-based detection methods such as Western blot, particularly for the detection of tubulin acetylation. Due to its low dynamic range, immunoblot analysis has limited sensitivity in detecting subtle changes in protein acetylation, while tubulin acetylation is influenced not only by HDAC6 but also other factors, including Sirt2, α-tubulin *N*-acetyltransferase (ATAT1), and oxidative stress.[40] Recently, the first NanoBRET HDAC6 target engagement assays using transfected cells overexpressing the nanoLuc-HDAC6 fusion gene were reported.[41,42] Nanoluciferase-based systems can be used to track protein levels and study protein interactions in living cells.[41,43–46] In NanoBRET target engagement assays, binding studies are typically conducted using cells that overexpress the target protein. However, perturbing the natural stoichiometry may cause problems such as aggregation and altered functions.[47,48] Furthermore, overexpression can affect protein localization and behavior, potentially leading to confounding results when studying protein-protein interactions, protein-ligand interactions, or protein dynamics under natural conditions. To mitigate this issues, it would be advantageous to use the endogenous promotor of the protein and maintain its natural expression level.[37,47] Schwinn *et al.* developed the HiBiT-LgBiT complementation technology, which enables the investigation of POIs in a native environment (Figure 1B).[47] The reconstituted nanoluciferase complex (Nluc) consists of an 11-amino acid tag (HiBiT) inserted at the C- or N-terminus of the POI by CRISP/Cas9 gene editing, and a larger subunit of 18 kDa (termed LgBiT). Co-expression of the POI-HiBiT and LgBiT within the same cell allows for the characterization of target engagement in a native endogenous environment.

Our group recently developed several PROTACs based on HDAC6 inhibitors.[23,49,50] In this work, we have therefore focused on establishing methods to investigate intracellular binary complex

formation between HDAC6 and PROTACs. Moreover, we have developed a method to precisely characterize the kinetics of PROTAC-induced HDAC6 degradation. Herein, we present a straightforward NanoBRET assay for studying cellular target engagement in a native environment, along with the development of an HDAC6 live cell kinetic degradation assay.

RESULTS AND DISCUSSION

Design, synthesis, and characterization of a fluorescent probe for HDAC6. For the development of a new NanoBRET assay for HDAC6 we first focused on the design and synthesis of suitable fluorescently labeled tracers. In previous research on NanoBRET tracers for chemokine receptors, we have successfully utilized cell-permeable TAMRA-based fluorophores, which are commonly used as acceptor fluorophores in NanoBRET assays.[51–55] We planned to introduce the TAMRA fluorophore by a Cu(I) catalyzed Huisgen 1,3-cycloaddition. To verify an appropriately positioned triazole as a suitable connecting unit between the HDACi and TAMRA, we conducted docking studies using the crystal structure of human HDAC6 (PDB: 5EDU). We utilized the hydroxamic acid substructure of vorinostat from the co-crystal structure of *Danio rerio* HDAC6 (PDB: 5EEI) as a template. This substructure was aligned with the human HDAC6 crystal structure to achieve a proper complexation of the zinc ion. Our docking studies with the ligand−triazole conjugate **1** (Figure 2A) indicated a binding mode similar to the parent ligand vorinostat (Figure 2A), i.e. occupying the L1 loop. Additionally, the ethyl-substituted triazole appears to be sufficiently solvent-exposed to serve as an exit vector for fluorophore installation.

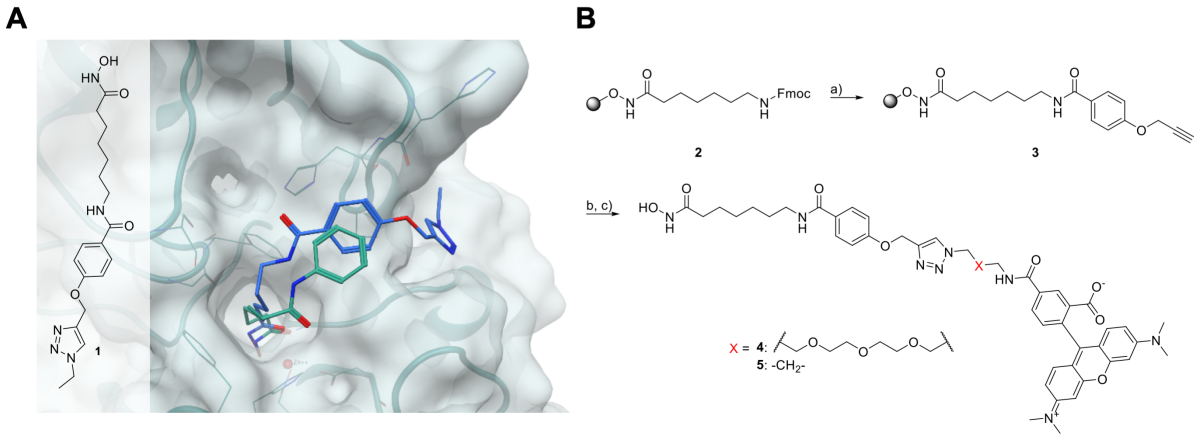

Figure 2. Development of fluorescent ligands for the HDAC6 NanoBRET assay. **A**: Predicted binding mode of the ligand−triazole conjugate **1** (blue colored) in human HDAC6 (PDB: 5EDU). X-ray conformation of vorinostat (turquoise colored) from *Danio rerio* HDAC6 (PDB: 5EEI) placed in human HDAC6 (PDB: 5EDU) *via* superposition. **B**: Synthesis of the TAMRA-based fluorescent HDAC ligands. *Reagents and conditions*: loading of resin **2**: 0.687 mmol/g; (a) (i) 20% piperidine, DMF, rt, 2 x 5 min, (ii) 4-(prop-2-yn-1-yloxy)benzoic acid, HATU, HOBt*H_2O, DIPEA, DMF, rt, 20 h; (b) azido-functionalized TAMRA analog, TBTA, $CuSO_4$*$5H_2O$, ascorbic acid, *t*-BuOH, DMF, rt, 18 h; (c) 5% TFA, 5% TIPS, CH_2Cl_2, rt, 1 h.

Since the linker length and type can influence cell permeability and fluorescence properties, we designed two different NanoBRET tracers. Compound **4** contains a PEG linker between TAMRA and the triazole connecting unit, while tracer **5** utilizes a shorter propylene linker. The synthesis of both tracers started from our previously published preloaded solid-phase resin HAIR D[56] (**2**) and is summarized in Figure 2B. In the first step, the Fmoc-protecting group was removed by treatment with piperidine. Subsequently, the HDACi cap was installed using a HATU-mediated amide coupling reaction, yielding the resin-bound intermediate **3** with a *para*-propargyloxy handle. The synthesis of the desired tracers was finalized by performing an on-resin Cu(I)-catalyzed Huisgen cycloaddition reaction with the respective azido-functionalized TAMRA analog, followed by cleavage from the solid support. Both tracers were further purified by preparative RP-HPLC to >95% purity.

Development of a NanoBRET HDAC6 target engagement assay. To evaluate the inhibitory activity and specificity of the fluorescently labelled ligands **4** and **5** for HDAC6, we initially characterized their binding properties in fluorogenic assays. The biochemical HDAC inhibition

assays confirmed that tracers **4** and **5** bind to HDAC1, HDAC2, and HDAC6 with both exhibiting the greatest inhibitory activity against HDAC6 (**4**: IC_{50} = 0.018 µM, **5:** IC_{50} = 0.0091 µM). The inhibitory activity against HDAC6 exceeded that of vorinostat (IC_{50} = 0.034 µM) (Table 1).

Table 1. In vitro inhibition of HDAC1, HDAC2, and HDAC6 by tracers **4** and **5**.

	IC_{50} ± SD (µM)[a]		
	HDAC1	HDAC2	HDAC6
4	0.20 ± 0.02	0.34 ± 0.04	0.018 ± 0.001
5	0.13 ± 0.02	0.22 ± 0.01	0.0091 ± 0.0001
vorinostat	0.15 ± 0.02	0.25 ± 0.01	0.034 ± 0.003

[a]Mean ± SD, duplicate measurement, n ≥ 2.

In the second step, we developed a NanoBRET-based binding assay (see Figure 3A for a schematic representation). To this end, we investigated the affinity of tracers **4** and **5** (see Figure 3B for extinction and emission spectra of **5**) for HDAC6 in $HeLa^{HDAC6\text{-}HiBiT}$ cells stably expressing the LgBiT protein. In whole cell assays, both tracers showed K_d values in the sub-micromolar concentration range (**4**: K_d = 0.12 ± 0.04 µM, **5**: K_d = 0.080 ± 0.011 µM, Figure 3C and D). To assess cell permeability, we permeabilized cells with digitonin and found a lower K_d value for **4** (K_d = 0.046 ± 0.021 µM), while the K_d value for **5** remained unchanged (K_d = 0.080 ± 0.011 µM). Since tracer **5** demonstrated higher affinity for HDAC6 and favorable cell permeability, we selected it for the subsequent displacement experiments.

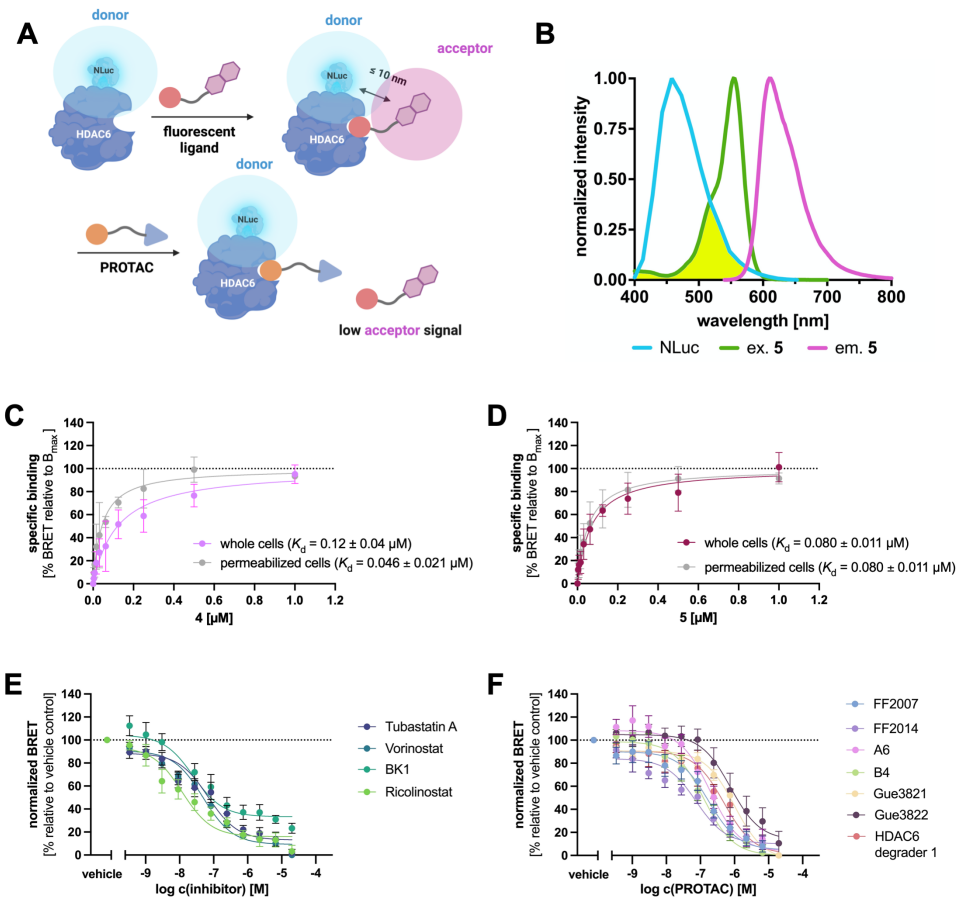

Figure 3. Development of a novel NanoBRET assay for HDAC6 target engagement studies in HeLa$^{\text{HDAC6-HiBiT}}$ cells stably expressing the LgBiT protein. **A**: Schematic presentation of the NanoBRET strategy to detect the binding to HDAC6 in cells. **B**: Bioluminescence spectrum of NLuc (blue line) and excitation (green) and emission (pink) spectra of the TAMRA-labeled inhibitor **5**. Energy transfer from NLuc to the tracer fluorophore is detectable through its emission spectrum. The data are normalized to the respective maximum of each spectrum. **C-D**: Specific saturation binding curves of **4** (**C**) and **5** (**D**) in a NanoBRET assay in whole cells and after permeabilization with digitonin (50 µg/mL) (mean ± SEM, duplicate measurement, n ≥ 3). **E-F**: Competition binding curves of inhibitors (**E**) and PROTACs (**F**) obtained with **5** (500 nM) in whole cells normalized to vehicle control and unspecific binding (mean ± SEM, duplicate measurement,

n ≥ 3). Compounds Gue3821 and HDAC6 degrader 1 exhibit autofluorescence at higher concentrations; curves were adjusted to unspecific binding.

In a third step, we evaluated compound **5** as a fluorescent probe to investigate HDAC6 target engagement in whole cells. We evaluated a set of HDAC inhibitors (vorinostat, ricolinostat, tubastatin A, and BK1) and recently published PROTACs in competition binding experiments (Figure 4).[23,50,57,58] For the PROTACs, compounds were selected to represent a diverse range of scaffolds, including both non-selective vorinostat-like and selective HDAC6-targeting warheads. Two types of zinc-binding groups (ZBGs) were incorporated: hydroxamic acids and difluoromethyl-1,3,4-oxadiazoles (DFMOs). The E3 ligase ligands used were well-established recruiters of cereblon (CRBN) and von Hippel–Lindau (VHL).

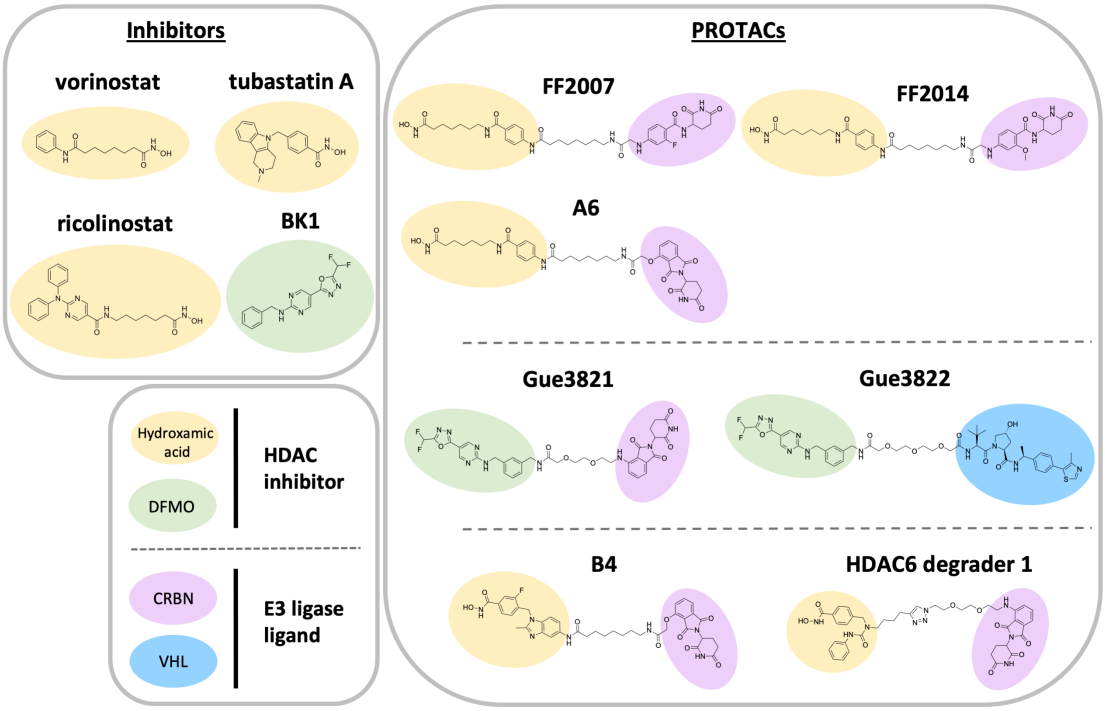

Figure 4. Structures of HDAC inhibitors and PROTACs used in this study. DFMO: difluoromethyl-1,3,4-oxadiazole, CRBN: cereblon, VHL: von Hippel-Lindau.

For the displacement assays, tracer **5** was used at a concentration of 500 nM. The results are shown in Figure 3E, F and Table 2. Compounds Gue3821 and HDAC6 degrader 1 exhibited autofluorescence at higher concentrations (≥ 2.34 µM), which interfered with the NanoBRET signal, as previously reported for other pomalidomide derivatives.[49,59] Therefore, the calculated IC_{50} values for these compounds represent an upper estimate. Among the HDAC inhibitors, ricolinostat exhibited the highest potency in displacing tracer **5** (IC_{50} = 0.021 ± 0.011 µM). Surprisingly, tubastatin A showed the lowest potency in the NanoBRET assay (IC_{50} = 0.091 ± 0.024 µM), but demonstrated stronger target engagement than previously reported in an overexpressing cell system using a different fluorescent tracer.[41] Notably, tubastatin A exhibited the highest potency in the biochemical HDAC6 inhibition assay (Table 2).

Table 2. NanoBRET binding results obtained with tracer **5** (500 nM).

	HDAC6 enzyme inhibition	**NanoBRET assay**[a]	
	IC_{50} ± SD (µM)	**IC_{50} ± SEM (µM)**	**K_i ± SEM (µM)**
tubastatin A	0.014 ± 0.001[60]	0.091 ± 0.024	0.011 ± 0.004
vorinostat	0.034 ± 0.003	0.046 ± 0.008	0.0057 ± 0.0010
BK1	0.19 ± 0.01[61]	0.075 ± 0.030	n.d.
ricolinostat	0.018 ± 0.003[60]	0.021 ± 0.011	0.0015 ± 0.0008
FF2007	0.0068 ± 0.0005	0.17 ± 0.04	0.025 ± 0.005
FF2014	0.0051 ± 0.0009	0.14 ± 0.06	0.015 ± 0.004
A6	0.0047 ± 0.0003[23]	0.23 ± 0.06	0.030 ± 0.008
B4	0.0045 ± 0.0004[23]	0.15 ± 0.05	0.021 ± 0.008
Gue3821	0.64 ± 0.21[50]	1.0 ± 0.2[b]	n.d.[c]
Gue3822	0.69 ± 0.12[50]	0.82 ± 0.16	n.d.[c]
HDAC6 degrader 1	0.026 ± 0.002	0.59 ± 0.21[b]	0.083 ± 0.030[b]

[a]IC_{50} values were calculated from competition binding curves (mean ± SEM, duplicate measurement, n ≥ 3). [b]Compounds showing autofluorescence at higher concentrations; curves were adjusted to unspecific binding. [c]n.d.: not determined, K_i values were calculated for the compounds that fulfill the criteria defined by the Cheng-Prusoff equation.

The results for the PROTACs are presented in Figure 3F and Table 2. Structurally, some PROTACs share common features, including similar scaffolds and linkers. Compounds FF2007, FF2014, and A6 have the same vorinostat-like HDAC scaffold and a cognate linker.[23,57] Interestingly, A6 displayed a higher IC_{50} value (IC_{50} = 0.23 ± 0.06 μM) in the NanoBRET assay than FF2007 and FF2014, although these compounds evoke similar HDAC6 inhibition in the enzymatic assay. Compounds Gue3821 and Gue3822, both based on the slow-binding selective HDAC6 inhibitor BK1[50] utilizing a difluoromethyl-1,3,4-oxadiazole (DFMO) ZBG, exhibited higher IC_{50} values in the displacement assays (Gue3821: IC_{50} = 1.0 ± 0.2 μM, Gue3822: IC_{50} = 0.82 ± 0.16 μM). The well-established reference PROTAC HDAC6 degrader 1[8] showed a moderate IC_{50} value in the NanoBRET assay (IC_{50} = 0.59 ± 0.21 μM) and also in the enzymatic HDAC6 inhibition assay.

In addition to the IC_{50} values for the HDAC inhibitors and the PROTACs, we also calculated the K_i values for the compounds meeting the criteria defined by the Cheng-Prusoff equation (Table 2).[62] Unlike the IC_{50} values from the displacement assay, which are highly dependent on assay conditions, the equilibrium dissociation constant (K_i) values calculated using the Cheng-Prusoff equation are system independent. The tracer concentration present in the medium was used for the calculation of K_i. Since BK1 inhibits HDAC6 through a distinct two-step slow binding mechanism that falls outside the criteria defined by the Cheng-Prusoff equation, this may also apply for the

derived PROTACs (Gue3821 and Gue3822). Therefore, K_i values were not calculated for these compounds.

Our results from the NanoBRET target engagement assay with endogenous HDAC6 expression confirmed the NanoBRET assay to be a suitable method for studying target engagement and binary complex formation between HDAC6 and PROTACs. Furthermore, these results suggest that the enzymatic assay may not necessarily be a reliable indicator of target engagement potency in a native environment.

Development of a kinetic live-cell HDAC6 degradation assay. To establish the HiBiT live cell kinetic system for characterizing our set of HDAC6-targeting PROTACs (Figure 4) in a native environment, and to detect HDAC6 degradation (see Figure 5A for a schematic representation of the assay principle), we first conducted an initial screening using immunoblotting analysis. This screening was performed in $HeLa^{HDAC6\text{-}HiBiT}$ cells stably expressing the LgBiT protein and MM.1S cells (Figure 5B, Figure S1). In the next step, we evaluated the HDAC6 degradation using the lytic HiBiT detection assay in $HeLa^{HDAC6\text{-}HiBiT}$ cells stably expressing the LgBiT protein (Figure 5C). Western blot analysis revealed higher HDAC6 degradation in MM.1S cells compared to $HeLa^{HDAC6\text{-}HiBiT}$ cells, suggesting the degradation efficiency to be cell line-dependent. Despite the less efficient degradation was observed in $HeLa^{HDAC6\text{-}HiBiT}$ cells, a strong correlation was found between the results of the immunoblot analysis and the lytic HiBiT detection assay (24 h: $r^2 = 0.98$, slope = 1.03) in $HeLa^{HDAC6\text{-}HiBiT}$ cells (Figure S2).

Next, we monitored the degradation kinetics for HDAC6 using the HiBiT live cell kinetic assay in $HeLa^{HDAC6\text{-}HiBiT}$ cells stably expressing LgBiT. The kinetic data are presented in Figure 5D-F and are consistent with the results from the immunoblot and the lytic HiBiT detection assays. Cell viability was assessed at the endpoint of the kinetic assay to rule out potential toxicity issues (Figure S3).

To better understand the differences in degradation kinetics among the PROTACs (see Table 3 for degradation rates, Dmax and $Dmax_{50}$ values, see Supporting Information for details), we examined their structural features in detail. First, we inspected compounds Gue3821 and Gue3822, both based on the slow-binding DFMO-based inhibitor BK1. Although Gue3821 (a CRBN recruiter) showed slightly more efficient degradation than Gue3822 (a VHL recruiter), both compounds exhibited the weakest HDAC6 degradation among this set of PROTACs. Their degradation followed almost

linear kinetics, with a hook effect observed at 5 μM. At higher concentrations, the degradation rates of both Gue3821 and Gue3822 also decreased, likely due to the hook effect. DFMO-based inhibitors such as BK1 exhibited a two-step slow binding mechanism, which may also apply to Gue3821 and Gue3822.[63,64]

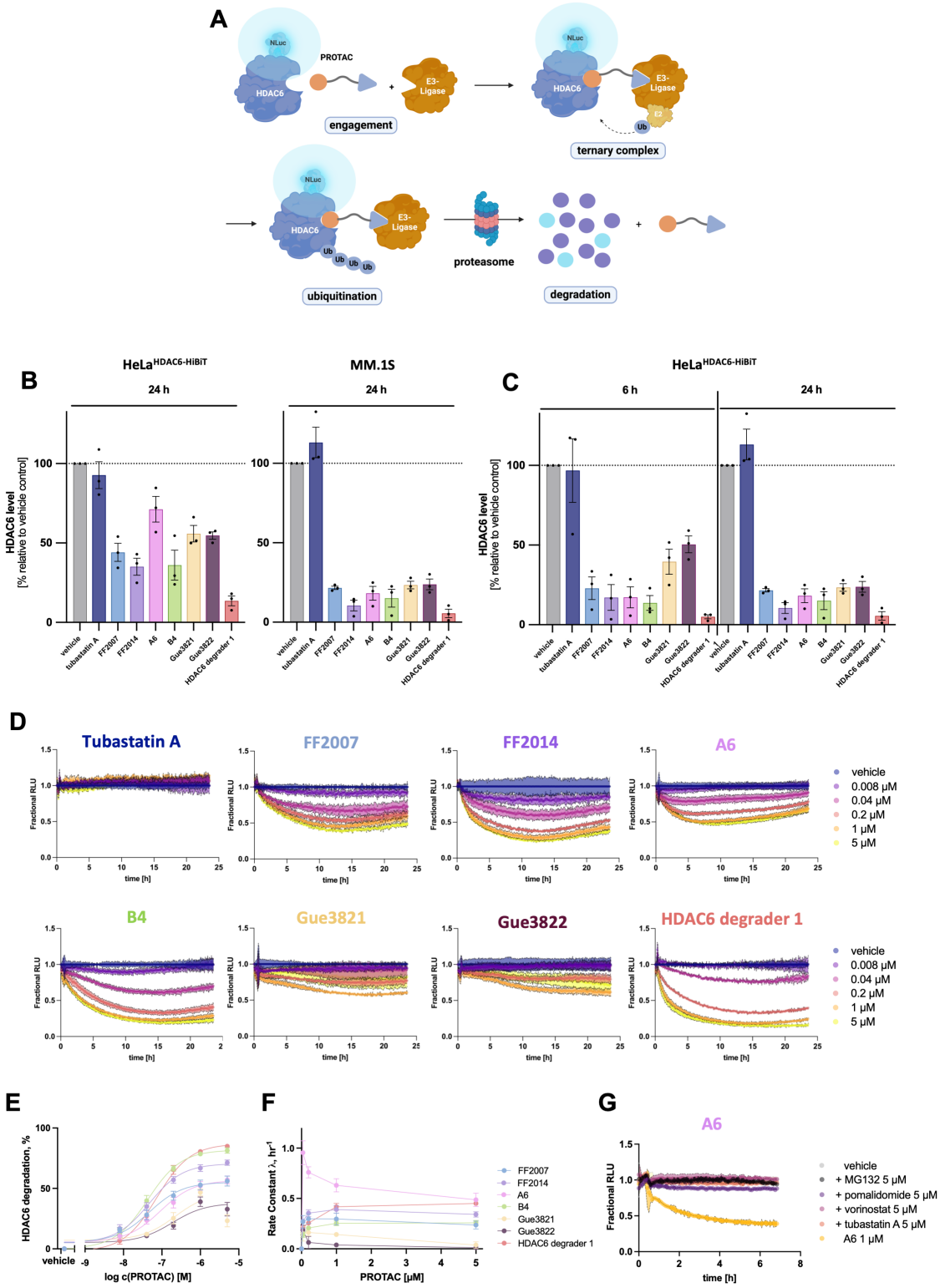

Figure 5. Development of a novel HiBiT live cell kinetic degradation assay. **A**: Schematic presentation of the HiBiT strategy to detect the degradation of HDAC6 in cells. **B-C**: Screening of

HDAC6 degradation after treatment with the PROTACs at 1 μM. **B**: Western Blot with HeLa$^{HDAC6-HiBiT}$ cells stably expressing the LgBiT protein and MM.1S cells with 1 μM of PROTACs after 24 h incubation (mean ± SEM, n = 3). **C**: HiBiT lytic detection with HDAC6 target engagement in HeLa$^{HDAC6-HiBiT}$ cells stably expressing the LgBiT protein with 1 μM after 6 h and 24 h incubation (mean ± SEM, triplicate measurement, n = 3). **D**: Live cell HDAC6 degradation kinetics for various PROTACs were assessed using the HiBiT live-cell degradation kinetic assay in HeLa$^{HDAC6-HiBiT}$ cells stably expressing the LgBiT protein. PROTACs were applied at the indicated concentrations for 24 hours (mean ± SD, triplicate measurement, n ≥ 3). RLU: relative light units. **E-F**: Determination of the $Dmax_{50}$ value (**E**), and degradation rate (**F**) (mean ± SEM, triplicate measurement, n ≥ 3). G: Rescue experiments were performed with MG132, pomalidomide, vorinostat, and tubastatin A at the indicated concentrations, using A6 as the representative PROTAC (mean ± SD, triplicate measurement, n = 2).

Next, the two most potent PROTACs B4[23] and HDAC6 degrader 1 were examined in detail. Interestingly, these compounds are structurally diverse, featuring different HDAC6 inhibitors, linker types, and linker lengths, but both share a similar CRBN recruiter. HDAC6 degrader 1 exhibited the highest potency and the fastest degradation. However, a comparison of the $Dmax_{50}$ revealed a lower $Dmax_{50}$ value for B4 ($Dmax_{50}$ = 0.044 ± 0.007 μM) than for HDAC6 degrader 1 ($Dmax_{50}$ = 0.077 ± 0.008 μM). We then analyzed the group consisting of FF2007, FF2014, and A6. All three compounds are based on the same pan-HDAC inhibitor scaffold and share an identical linker. A6 utilizes pomalidomide as a CRBN recruiter, while FF2007 and FF2014 use benzamide-based CRBN recruiters. Within this group, FF2014 was the most efficient degrader (at 5 μM: Dmax = 71 ± 3%) compared to FF2007 (at 5 μM: Dmax = 56 ± 5%) and A6 (at 5 μM: Dmax = 57 ± 4%). These results were in agreement with previously published data.[57] The $Dmax_{50}$ values of FF2007

($Dmax_{50}$ = 0.042 ± 0.006 μM) and FF2014 ($Dmax_{50}$ = 0.043 ± 0.006 μM) were highly similar. Interestingly, A6 showed a slight HDAC6 recovery over time, consistent with findings from a previous report using HiBiT-tagged K562 cells.[23] At high concentrations, A6 demonstrated a clear trend of a decelerating degradation rate (Figure 5F); however, the HDAC6 degradation provoked by A6 remained the fastest of all PROTACs tested. This decrease was not associated with a hook effect.

Finally, we successfully confirmed the dependence of HDAC6 degradation on ternary complex formation and the UPS using A6 as a representative example by co-treatment with MG132, pomalidomide, vorinostat, and tubastatin A (Figure 5G). While A6 alone induced a substantial reduction of HDAC6 protein levels, all co-treatment conditions resulted in a rescue of the A6-induced degradation. These data corroborated that A6-mediated HDAC6 degradation is UPS-dependent and requires binding to CRBN and HDAC6.

Taken together, our results demonstrate that the HDAC6 HiBiT live cell kinetic system in an endogenous environment is an effective tool for a rapid and in-depth elucidation of the degradation efficiency of PROTACs. The data presented provide valuable guidance for the optimization of structural features to improve PROTAC design targeting HDAC6. Furthermore, our results highlight the limitations of Western blotting, which lacks the sensitivity and dynamic range required to accurately measure subtle differences in the degradation performance of PROTACs.

Table 3. Calculation of the descriptive parameters of the HDAC6 degradation kinetics.

		Concentration (µM)[a]					Dmax$_{50}$ (µM)[a]
	Parameter	**0.008**	**0.04**	**0.2**	**1**	**5**	
FF2007	**Rate (hr^{-1})**	n.d.[b]	0.27 ± 0.07	0.30 ± 0.05	0.30 ± 0.06	0.24 ± 0.04	0.042 ± 0.006
	Dmax (%)	16 ± 3	28 ± 5	44 ± 5	53 ± 5	56 ± 5	
	AUC	22 ± 1	19 ± 2	16 ± 1	14 ± 1	14 ± 1	
FF2014	**Rate (hr^{-1})**	n.d.[b]	0.28 ± 0.02	0.35 ± 0.04	0.39 ± 0.04	0.34 ± 0.03	0.043 ± 0.006
	Dmax (%)	17 ± 4	35 ± 4	57 ± 3	67 ± 3	71 ± 3	
	AUC	21 ± 1	18 ± 1	13 ± 1	11 ± 1	9.8 ± 0.6	
A6	**Rate (hr^{-1})**	n.d.[b]	1.0 ± 0.2	0.76 ± 0.06	0.63 ± 0.07	0.49 ± 0.07	0.085 ± 0.028
	Dmax (%)	11 ± 3	24 ± 4	38 ± 5	52 ± 4	57 ± 4	
	AUC	23 ± 1	20 ± 2	17 ± 2	15 ± 2	13 ± 1	
B4	**Rate (hr^{-1})**	n.d.[b]	0.14 ± 0.03	0.21 ± 0.03	0.25 ± 0.03	0.26 ± 0.03	0.044 ± 0.007
	Dmax (%)	13 ± 4	40 ± 5	66 ± 3	79 ± 3	81 ± 3	
	AUC	22 ± 1	16 ± 1	11 ± 1	7.6 ± 0.3	7.0 ± 0.2	
Gue3821	**Rate (hr^{-1})**	n.d.[b]	0.15 ± 0.08	0.16 ± 0.04	0.14 ± 0.03	0.037 ± 0.032	0.23 ± 0.06[c]
	Dmax (%)	14 ± 5	12 ± 2	25 ± 5	47 ± 3	23 ± 5	
	AUC	22 ± 1	22 ± 1	19 ± 2	15 ± 1	20 ± 1	
Gue3822	**Rate (hr^{-1})**	n.d.[b]	0.19 ± 0.05	0.063 ± 0.060	0.039 ± 0.018	0.011 ± 0.007	0.16 ± 0.03
	Dmax (%)	11 ± 2	11 ± 1	19 ± 3	39 ± 4	33 ± 6	
	AUC	23 ± 1	23 ± 1	21 ± 1	17 ± 1	19 ± 2	
HDAC6 degrader 1	**Rate (hr^{-1})**	n.d.[b]	0.21 ± 0.02	0.26 ± 0.03	0.42 ± 0.04	0.45 ± 0.03	0.077 ± 0.008
	Dmax (%)	6.7 ± 2.9	27 ± 2	65 ± 4	80 ± 2	85 ± 2	
	AUC	23 ± 1	19 ± 1	11 ± 1	7.0 ± 0.6	5.8 ± 0.4	

[a]Mean ± SEM, triplicate measurement, n ≥ 3. [b]n.d. not determined, fitting not possible. [c]Hook effect at 5 µM, curve was adjusted to 1 µM.

CONCLUSION

The lack of robust tools to study cellular HDAC6 target engagement and degradation in a native environment has limited the progress in the field of targeted HDAC6 degraders. In this study, we developed tools to investigate HDAC6 target engagement and degradation in living cells and native environments. We applied the NanoBRET assay technology to detect binary complex formation of HDAC6 inhibitors and degraders with HDAC6 at an endogenous protein expression level. This method provides a better understanding of target-PROTAC interaction in native environments compared to the previously used approaches. In addition, we have established a live-cell assay to track the degradation of HDAC6 using the HiBiT-LgBiT complementation technology. Unlike traditional Western blot techniques, this kinetic assay overcomes the challenges of time and concentration variability by providing real-time insights. The resulting degradation profiles offer a range of key parameters for multidimensional analysis and provide insights into mechanistic aspects that can guide the optimization of PROTACs. Collectively, our findings will support future investigations on HDAC6 degradation, offer new perspectives on the mechanism of action of PROTACs, and will serve as a promising basis for future medicinal chemistry campaigns to design and discover effective HDAC6 degraders with high specificity and efficiency.

ASSOCIATED CONTENT

Supporting Information

Supplementary figures; experimental procedures; general information and chemistry; ^{1}H NMR and ^{13}C NMR spectra; HPLC data of newly synthesized compounds (PDF)

AUTHOR INFORMATION

Corresponding Author

F.K.H.: phone, (+49) 228 73 5213; E-mail, finn.hansen@uni-bonn.de.

ORCID

Maria Hanl: 0009-0002-1436-7607

Felix Feller: 0009-0007-1820-772X

Irina Honin: 0009-0009-7091-8419

Kathrin Tan: 0000-0003-0565-2676

Linda Schäker-Hübner: 0000-0001-7734-124X

Matthias Schiedel: 0000-0001-7365-3617

Michael Gütschow: 0000-0002-9376-7897

Gerd Bendas: 0000-0002-8667-7201

Finn K. Hansen: 0000-0001-9765-5975

Author Contributions

The manuscript was written through contributions of all authors. All authors have given approval to the final version.

Funding

The work of M.H., I.H., L.S.-H., M.G., G.B., and F.K.H. was funded by the Deutsche Forschungsgemeinschaft (DFG, German Research Foundation)–GRK2873 (494832089).

Notes

The authors declare no competing financial interest.

ACKNOWLEDGMENTS

Experimental support by Svenja Henze is gratefully acknowledged. The authors thank and Dr. Tim Keuler, Dr. Beate König, and Dr. Christian Steinebach for providing certain PROTACs and PROTAC building blocks. Figure 1, Figure 3, Figure 5, and the TOC graphic were created using Biorender.com

ABBREVIATIONS

ATAT1, *N*-acetyltransferase; AUC, area under the curve; BRET, bioluminescence resonance energy transfer; CD, catalytic domain; $CDCl_3$, chloroform-*d*; CRBN, cereblon; DCM, dichloromethane; DFMO, difluoromethyl-1,3,4-oxadiazole; DIPEA, *N*,*N*-diisopropylethylamine; Dmax, maximal degradation; $Dmax_{50}$, half maximal degradation at the timepoint of Dmax; DMB, dynein motor binding domain; DMF, *N*,*N*-dimethylformamide; DMSO, dimethylsulfoxide; EMA, European Medicines Agency; EtOAc, ethyl acetate; HAT, histone acetyltransferases; HATU, hexafluorophosphate azabenzotriazole tetramethyl uranium; HDAC, histone deacetylase; HDACi,

histone deacetylase inhibitor(s); HOBt*H_2O, hydroxybenzotriazole hydrate; HSF-1, heat shock factor protein 1; Hsp90, heat shock protein 90; IC_{50}, half maximal inhibitory concentration; MeOH, methanol; min, minutes; NAD^+, nicotinamide adenine dinucleotide; NES, nuclear export signal; NLS, nuclear localization signal; Nluc, nanoluciferase; PDB, protein data bank; POI, protein of interest; PROTAC, PROteolysis TArgeting Chimeras; RLU, relative light units; rt, room temperature; SD, standard deviation; SEM, standard error of the mean; SE14, serine-glutamate tetradecapeptide repeat; SIRT, sirtuin; *t*-BuOH, *tert*-butanol; TAMRA, tetramethylrhodamine; TBTA, tris(benzyltriazolylmethyl)amine; TFA, trifluoroacetic acid; TFMO, trifluoromethyl-1,3,4-oxadiazole; TIPS, triisopropylsilane; TPD, targeted protein degradation; UPS, ubiquitin-proteasome system; U.S. FDA, United States Food and Drug Administration; VHL, von Hippel-Lindau; ZnF-UBP, ubiquitin-binding zinc finger domain.

REFERENCES

(1) Choudhary, C.; Kumar, C.; Gnad, F.; Nielsen, M. L.; Rehman, M.; Walther, T. C.; Olsen, J. V.; Mann, M. Lysine Acetylation Targets Protein Complexes and Co-Regulates Major Cellular Functions. *Science* **2009**, *325* (5942), 834–840.

(2) Bradner, J. E.; West, N.; Grachan, M. L.; Greenberg, E. F.; Haggarty, S. J.; Warnow, T.; Mazitschek, R. Chemical Phylogenetics of Histone Deacetylases. *Nat. Chem. Biol.* **2010**, *6* (3), 238–243.

(3) Seto, E.; Yoshida, M. Erasers of Histone Acetylation: The Histone Deacetylase Enzymes. *Cold Spring Harb. Perspect. Biol.* **2014**, *6* (4), a018713.

(4) Ho, T. C. S.; Chan, A. H. Y.; Ganesan, A. Thirty Years of HDAC Inhibitors: 2020 Insight and Hindsight. *J. Med. Chem.* **2020**, *63* (21), 12460–12484.

(5) Li, Y.; Shin, D.; Kwon, S. H. Histone Deacetylase 6 Plays a Role as a Distinct Regulator of Diverse Cellular Processes. *FEBS J.* **2013**, *280* (3), 775–793.

(6) Zhu, Y.; Feng, M.; Wang, B.; Zheng, Y.; Jiang, D.; Zhao, L.; Mamun, M. A. A.; Kang, H.; Nie, H.; Zhang, X.; Guo, N.; Qin, S.; Wang, N.; Liu, H.; Gao, Y. New Insights into the Non-Enzymatic Function of HDAC6. *Biomed. Pharmacother.* **2023**, *161*, 114438.

(7) Pulya, S.; Amin, S. A.; Adhikari, N.; Biswas, S.; Jha, T.; Ghosh, B. HDAC6 as Privileged Target in Drug Discovery: A Perspective. *Pharmacol. Res.* **2021**, *163*, 105274.

(8) An, Z.; Lv, W.; Su, S.; Wu, W.; Rao, Y. Developing Potent PROTACs Tools for Selective Degradation of HDAC6 Protein. *Protein Cell* **2019**, *10* (8), 606–609.

(9) Liang, T.; Fang, H. Structure, Functions and Selective Inhibitors of HDAC6. *Curr. Top.*

Med. Chem. **2018**, *18* (28), 2429–2447.

(10) Zhang, X. H.; Qin-Ma; Wu, H. P.; Khamis, M. Y.; Li, Y. H.; Ma, L. Y.; Liu, H. M. A Review of Progress in Histone Deacetylase 6 Inhibitors Research: Structural Specificity and Functional Diversity. *J. Med. Chem.* **2021**, *64* (3), 1362–1391.

(11) Arrowsmith, C. H.; Bountra, C.; Fish, P. V.; Lee, K.; Schapira, M. Epigenetic Protein Families: A New Frontier for Drug Discovery. *Nat. Rev. Drug Discov.* **2012**, *11* (5), 384–400.

(12) Osko, J. D.; Christianson, D. W. Structural Basis of Catalysis and Inhibition of HDAC6 CD1, the Enigmatic Catalytic Domain of Histone Deacetylase 6. *Biochemistry* **2019**, *58* (49), 4912–4924.

(13) Hai, Y.; Christianson, D. W. Histone Deacetylase 6 Structure and Molecular Basis of Catalysis and Inhibition. *Nat. Chem. Biol.* **2016**, *12* (9), 741–747.

(14) Miyake, Y.; Keusch, J. J.; Wang, L.; Saito, M.; Hess, D.; Wang, X.; Melancon, B. J.; Helquist, P.; Gut, H.; Matthias, P. Structural Insights into HDAC6 Tubulin Deacetylation and Its Selective Inhibition. *Nat. Chem. Biol.* **2016**, *12* (9), 748–754.

(15) Hontecillas-Prieto, L.; Flores-Campos, R.; Silver, A.; de Álava, E.; Hajji, N.; García-Domínguez, D. J. Synergistic Enhancement of Cancer Therapy Using HDAC Inhibitors: Opportunity for Clinical Trials. *Front. Genet.* **2020**, *11*, 578011.

(16) Jenke, R.; Reßing, N.; Hansen, F. K.; Aigner, A.; Büch, T. Anticancer Therapy with HDAC Inhibitors: Mechanism-Based Combination Strategies and Future Perspectives. *Cancers (Basel)*. **2021**, *13* (4), 634.

(17) Lee, H. Z.; Kwitkowski, V. E.; Del Valle, P. L.; Ricci, M. S.; Saber, H.; Habtemariam, B.

A.; Bullock, J.; Bloomquist, E.; Shen, Y. L.; Chen, X. H.; Brown, J.; Mehrotra, N.; Dorff, S.; Charlab, R.; Kane, R. C.; Kaminskas, E.; Justice, R.; Farrell, A. T.; Pazdur, R. FDA Approval: Belinostat for the Treatment of Patients with Relapsed or Refractory Peripheral T-Cell Lymphoma. *Clin. Cancer Res.* **2015**, *21* (12), 2666–2670.

(18) Mann, B. S.; Johnson, J. R.; Cohen, M. H.; Justice, R.; Pazdur, R. FDA Approval Summary: Vorinostat for Treatment of Advanced Primary Cutaneous T-Cell Lymphoma. *Oncologist* **2007**, *12* (10), 1247–1252.

(19) Frye, R.; Myers, M.; Axelrod, K. C.; Ness, E. A.; Piekarz, R. L.; Bates, S. E.; Booher, S. Romidepsin: A New Drug for the Treatment of Cutaneous T-Cell Lymphoma. *Clin. J. Oncol. Nurs.* **2012**, *16* (2), 195–204.

(20) Mercuri, E.; Vilchez, J. J.; Boespflug-Tanguy, O.; Zaidman, C. M.; Mah, J. K.; Goemans, N.; Müller-Felber, W.; Niks, E. H.; Schara-Schmidt, U.; Bertini, E.; Comi, G. P.; Mathews, K. D.; Servais, L.; Vandenborne, K.; Johannsen, J.; Messina, S.; Spinty, S.; McAdam, L.; Selby, K.; Byrne, B.; Laverty, C. G.; Carroll, K.; Zardi, G.; Cazzaniga, S.; Coceani, N.; Bettica, P.; McDonald, C. M. Safety and Efficacy of Givinostat in Boys with Duchenne Muscular Dystrophy (EPIDYS): A Multicentre, Randomised, Double-Blind, Placebo-Controlled, Phase 3 Trial. *Lancet Neurol.* **2024**, *23* (4), 393–403.

(21) Eleutherakis-Papaiakovou, E.; Kanellias, N.; Kastritis, E.; Gavriatopoulou, M.; Terpos, E.; Dimopoulos, M. A. Efficacy of Panobinostat for the Treatment of Multiple Myeloma. *J. Oncol.* **2020**, *2020* (1), 713802.

(22) Huang, Z.; Li, L.; Cheng, B.; Li, D. Small Molecules Targeting HDAC6 for Cancer Treatment: Current Progress and Novel Strategies. *Biomed. Pharmacother.* **2024**, *178*, 117218.

(23) Sinatra, L.; Yang, J.; Schliehe-Diecks, J.; Dienstbier, N.; Vogt, M.; Gebing, P.; Bachmann, L. M.; Sönnichsen, M.; Lenz, T.; Stühler, K.; Schöler, A.; Borkhardt, A.; Bhatia, S.; Hansen, F. K. Solid-Phase Synthesis of Cereblon-Recruiting Selective Histone Deacetylase 6 Degraders (HDAC6 PROTACs) with Antileukemic Activity. *J. Med. Chem.* **2022**, *65* (24), 16860–16878.

(24) Wu, T.; Yoon, H.; Xiong, Y.; Dixon-Clarke, S. E.; Nowak, R. P.; Fischer, E. S. Targeted Protein Degradation as a Powerful Research Tool in Basic Biology and Drug Target Discovery. *Nat. Struct. Mol. Biol.* **2020**, *27* (7), 605–614.

(25) Churcher, I. Protac-Induced Protein Degradation in Drug Discovery: Breaking the Rules or Just Making New Ones? *J. Med. Chem.* **2018**, *61* (2), 444–452.

(26) Wang, X.; Qin, Z. L.; Li, N.; Jia, M. Q.; Liu, Q. G.; Bai, Y. R.; Song, J.; Yuan, S.; Zhang, S. Y. Annual Review of PROTAC Degraders as Anticancer Agents in 2022. *Eur. J. Med. Chem.* **2024**, *267*, 116166.

(27) Hamilton, E. P.; Ma, C.; Laurentiis, M. De; Iwata, H.; Hurvitz, S. A.; Wander, S. A.; Danso, M.; Lu, D. R.; Smith, J. P.; Liu, Y.; Tran, L.; Anderson, S.; Campone, M. VERITAC-2: A Phase III Study of Vepdegestrant, a PROTAC ER Degrader, versus Fulvestrant in ER+/HER2- Advanced Breast Cancer. *Futur. Oncol.* **2024**, *20* (32), 2447–2455.

(28) Pettersson, M.; Crews, C. M. PROteolysis TArgeting Chimeras (PROTACs) — Past, Present and Future. *Drug Discov. Today Technol.* **2019**, *31*, 15–27.

(29) Smith, B. E.; Wang, S. L.; Jaime-Figueroa, S.; Harbin, A.; Wang, J.; Hamman, B. D.; Crews, C. M. Differential PROTAC Substrate Specificity Dictated by Orientation of Recruited E3 Ligase. *Nat. Commun.* **2019**, *10* (1), 1–13.

(30) Békés, M.; Langley, D. R.; Crews, C. M. PROTAC Targeted Protein Degraders: The Past Is Prologue. *Nat. Rev. Drug Discov.* **2022**, *21* (3), 181–200.

(31) Lai, A. C.; Crews, C. M. Induced Protein Degradation: An Emerging Drug Discovery Paradigm. *Nat. Rev. Drug Discov.* **2017**, *16* (2), 101–114.

(32) Casement, R.; Bond, A.; Craigon, C.; Ciulli, A. Mechanistic and Structural Features of PROTAC Ternary Complexes. In *Targeted Protein Degradation*; 2021; pp 79–113.

(33) Riching, K. M.; Caine, E. A.; Urh, M.; Daniels, D. L. The Importance of Cellular Degradation Kinetics for Understanding Mechanisms in Targeted Protein Degradation. *Chem. Soc. Rev.* **2022**, *51* (14), 6210–6221.

(34) Němec, V.; Schwalm, M. P.; Müller, S.; Knapp, S. PROTAC Degraders as Chemical Probes for Studying Target Biology and Target Validation. *Chem. Soc. Rev.* **2022**, *51* (18), 7971–7993.

(35) Bondeson, D. P.; Smith, B. E.; Burslem, G. M.; Buhimschi, A. D.; Hines, J.; Jaime-Figueroa, S.; Wang, J.; Hamman, B. D.; Ishchenko, A.; Crews, C. M. Lessons in PROTAC Design from Selective Degradation with a Promiscuous Warhead. *Cell Chem. Biol.* **2018**, *25* (1), 78-87.e5.

(36) Wurz, R. P.; Rui, H.; Dellamaggiore, K.; Ghimire-Rijal, S.; Choi, K.; Smither, K.; Amegadzie, A.; Chen, N.; Li, X.; Banerjee, A.; Chen, Q.; Mohl, D.; Vaish, A. Affinity and Cooperativity Modulate Ternary Complex Formation to Drive Targeted Protein Degradation. *Nat. Commun.* **2023**, *14* (1), 4177.

(37) Paiva, S. L.; Crews, C. M. Targeted Protein Degradation: Elements of PROTAC Design. *Curr. Opin. Chem. Biol.* **2019**, *50*, 111–119.

(38) He, S.; Dong, G.; Cheng, J.; Wu, Y.; Sheng, C. Strategies for Designing Proteolysis Targeting Chimaeras (PROTACs). *Med. Res. Rev.* **2022**, *42* (3), 1280–1342.

(39) Stefaniak, J.; Huber, K. V. M. Importance of Quantifying Drug-Target Engagement in Cells. *ACS Med. Chem. Lett.* **2020**, *11* (4), 403–406.

(40) Vogelmann, A.; Jung, M.; Hansen, F. K.; Schiedel, M. Comparison of Cellular Target Engagement Methods for the Tubulin Deacetylases Sirt2 and HDAC6: NanoBRET, CETSA, Tubulin Acetylation, and PROTACs. *ACS Pharmacol. Transl. Sci.* **2022**, *5* (2), 138–140.

(41) Ptacek, J.; Snajdr, I.; Schimer, J.; Kutil, Z.; Mikesova, J.; Baranova, P.; Havlinova, B.; Tueckmantel, W.; Majer, P.; Kozikowski, A.; Barinka, C. Selectivity of Hydroxamate- and Difluoromethyloxadiazole-Based Inhibitors of Histone Deacetylase 6 In Vitro and in Cells. *Int. J. Mol. Sci.* **2023**, *24* (5), 4720.

(42) Morgen, M.; Steimbach, R. R.; Géraldy, M.; Hellweg, L.; Sehr, P.; Ridinger, J.; Witt, O.; Oehme, I.; Herbst-Gervasoni, C. J.; Osko, J. D.; Porter, N. J.; Christianson, D. W.; Gunkel, N.; Miller, A. K. Design and Synthesis of Dihydroxamic Acids as HDAC6/8/10 Inhibitors. *ChemMedChem* **2020**, *15* (13), 1163–1174.

(43) Vogelmann, A.; Schiedel, M.; Wössner, N.; Merz, A.; Herp, D.; Hammelmann, S.; Colcerasa, A.; Komaniecki, G.; Hong, J.; Sum, M.; Metzger, E.; Neuwirt, E.; Zhang, L.; Einsle, O.; Groß, O.; Schüle, R.; Lin, H.; Sippl, W.; Jung, M. Development of a NanoBRET Assay to Validate Inhibitors of Sirt2-Mediated Lysine Deacetylation and Defatty-Acylation That Block Prostate Cancer Cell Migration. *RSC Chem. Biol.* **2022**, *3* (4), 468–485.

(44) Schwalm, M. P.; Krämer, A.; Dölle, A.; Weckesser, J.; Yu, X.; Jin, J.; Saxena, K.; Knapp,

S. Tracking the PROTAC Degradation Pathway in Living Cells Highlights the Importance of Ternary Complex Measurement for PROTAC Optimization. *Cell Chem. Biol.* **2023**, *30* (7), 753-765.e8.

(45) Dölle, A.; Adhikari, B.; Krämer, A.; Weckesser, J.; Berner, N.; Berger, L. M.; Diebold, M.; Szewczyk, M. M.; Barsyte-Lovejoy, D.; Arrowsmith, C. H.; Gebel, J.; Löhr, F.; Dötsch, V.; Eilers, M.; Heinzlmeir, S.; Kuster, B.; Sotriffer, C.; Wolf, E.; Knapp, S. Design, Synthesis, and Evaluation of WD-Repeat-Containing Protein 5 (WDR5) Degraders. *J. Med. Chem.* **2021**, *64* (15), 10682–10710.

(46) Daniels, D. L.; Riching, K. M.; Urh, M. Monitoring and Deciphering Protein Degradation Pathways inside Cells. *Drug Discov. Today Technol.* **2019**, *31*, 61–68.

(47) Schwinn, M. K.; Steffen, L. S.; Zimmerman, K.; Wood, K. V.; Machleidt, T. A Simple and Scalable Strategy for Analysis of Endogenous Protein Dynamics. *Sci. Rep.* **2020**, *10*, 8953.

(48) Moriya, H. Quantitative Nature of Overexpression Experiments. *Mol. Biol. Cell* **2015**, *26* (22), 3932–3939.

(49) Zhai, S.; Schäker-Hübner, L.; Hanl, M.; Jacobi, L.; Pieńkowska, D. E.; Gerhartz, J.; Voget, R.; Gütschow, M.; Meissner, F.; Nowak, R. P.; Steinebach, C.; Hansen, F. K. Development and Characterization of the First Selective Class IIb Histone Deacetylase Degraders. *ChemRxiv* **2024**, DOI: 10.26434/chemrxiv-2024-ngppg-v2.

(50) Keuler, T.; König, B.; Bückreiß, N.; Kraft, F. B.; König, P.; Schäker-Hübner, L.; Steinebach, C.; Bendas, G.; Gütschow, M.; Hansen, F. K. Development of the First Non-Hydroxamate Selective HDAC6 Degraders. *Chem. Commun.* **2022**, *58* (79), 11087–11090.

(51) Wurnig, S. L.; Huber, M. E.; Weiler, C.; Baltrukevich, H.; Merten, N.; Stötzel, I.; Steffen,

T.; Chang, Y.; Klammer, R. H. L.; Baumjohann, D.; Kiermaier, E.; Kolb, P.; Kostenis, E.; Schiedel, M.; Hansen, F. K. A Fluorescent Probe Enables the Discovery of Improved Antagonists Targeting the Intracellular Allosteric Site of the Chemokine Receptor CCR7. *J. Med. Chem.* **2025**, *68* (4), 4308–4333.

(52) Huber, M. E.; Wurnig, S.; Toy, L.; Weiler, C.; Merten, N.; Kostenis, E.; Hansen, F. K.; Schiedel, M. Fluorescent Ligands Enable Target Engagement Studies for the Intracellular Allosteric Binding Site of the Chemokine Receptor CXCR2. *J. Med. Chem.* **2023**, *66* (14), 9916–9933.

(53) Huber, M. E.; Toy, L.; Schmidt, M. F.; Vogt, H.; Budzinski, J.; Wiefhoff, M. F. J.; Merten, N.; Kostenis, E.; Weikert, D.; Schiedel, M. A Chemical Biology Toolbox Targeting the Intracellular Binding Site of CCR9: Fluorescent Ligands, New Drug Leads and PROTACs. *Angew. Chem. Int. Ed.* **2022**, *61* (12), e202116782.

(54) Toy, L.; Huber, M. E.; Schmidt, M. F.; Weikert, D.; Schiedel, M. Fluorescent Ligands Targeting the Intracellular Allosteric Binding Site of the Chemokine Receptor CCR2. *ACS Chem. Biol.* **2022**, *17* (8), 2142–2152.

(55) Rosier, N.; Grätz, L.; Schihada, H.; Möller, J.; Işbilir, A.; Humphrys, L. J.; Nagl, M.; Seibel, U.; Lohse, M. J.; Pockes, S. A Versatile Sub-Nanomolar Fluorescent Ligand Enables NanoBRET Binding Studies and Single-Molecule Microscopy at the Histamine H3Receptor. *J. Med. Chem.* **2021**, *64* (15), 11695–11708.

(56) Sinatra, L.; Bandolik, J. J.; Roatsch, M.; Sönnichsen, M.; Schoeder, C. T.; Hamacher, A.; Schöler, A.; Borkhardt, A.; Meiler, J.; Bhatia, S.; Kassack, M. U.; Hansen, F. K. Hydroxamic Acids Immobilized on Resins (HAIRs): Synthesis of Dual-Targeting HDAC Inhibitors and HDAC Degraders (PROTACs). *Angew. Chem. Int. Ed.* **2020**, *59* (50), 22494–22499.

(57) Steinebach, C.; Bricelj, A.; Murgai, A.; Sosič, I.; Bischof, L.; Ng, Y. L. D.; Heim, C.; Maiwald, S.; Proj, M.; Voget, R.; Feller, F.; Košmrlj, J.; Sapozhnikova, V.; Schmidt, A.; Zuleeg, M. R.; Lemnitzer, P.; Mertins, P.; Hansen, F. K.; Gütschow, M.; Krönke, J.; Hartmann, M. D. Leveraging Ligand Affinity and Properties: Discovery of Novel Benzamide-Type Cereblon Binders for the Design of PROTACs. *J. Med. Chem.* **2023**, *66* (21), 14513–14543.

(58) Yang, K.; Song, Y.; Xie, H.; Wu, H.; Wu, Y. T.; Leisten, E. D.; Tang, W. Development of the First Small Molecule Histone Deacetylase 6 (HDAC6) Degraders. *Bioorg. Med. Chem. Lett.* **2018**, *28* (14), 2493–2497.

(59) Nowak, R. P.; Ragosta, L.; Huerta, F.; Liu, H.; Ficarro, S. B.; Cruite, J. T.; Metivier, R. J.; Donovan, K. A.; Marto, J. A.; Fischer, E. S.; Zerfas, B. L.; Jones, L. H. Development of a Covalent Cereblon-Based PROTAC Employing a Fluorosulfate Warhead. *RSC Chem. Biol.* **2023**, *4* (11), 906–912.

(60) Mackwitz, M. K. W.; Hamacher, A.; Osko, J. D.; Held, J.; Schöler, A.; Christianson, D. W.; Kassack, M. U.; Hansen, F. K. Multicomponent Synthesis and Binding Mode of Imidazo[1,2- a]Pyridine-Capped Selective HDAC6 Inhibitors. *Org. Lett.* **2018**, *20* (11), 3255–3258.

(61) König, B.; Watson, P. R.; Reßing, N.; Cragin, A. D.; Schäker-Hübner, L.; Christianson, D. W.; Hansen, F. K. Difluoromethyl-1,3,4-Oxadiazoles Are Selective, Mechanism-Based, and Essentially Irreversible Inhibitors of Histone Deacetylase 6. *J. Med. Chem.* **2023**, *66* (19), 13821–13837.

(62) Cheng, Y.-C.; Prusoff, W. H. Relationship between the Inhibition Constant (Ki) and the Concentration of Inhibitor Which Causes 50 per Cent Inhibition (I50) of an Enzymatic

Reaction. *Biochem. Pharmacol.* **1973**, *22* (23), 3099–3108.

(63) Cellupica, E.; Caprini, G.; Fossati, G.; Mirdita, D.; Cordella, P.; Marchini, M.; Rocchio, I.; Sandrone, G.; Stevenazzi, A.; Vergani, B.; Steinkühler, C.; Vanoni, M. A. The Importance of the "Time Factor" for the Evaluation of Inhibition Mechanisms: The Case of Selected HDAC6 Inhibitors. *Biology (Basel).* **2023**, *12* (8), 1049.

(64) König, B.; Watson, P. R.; Reßing, N.; Cragin, A. D.; Schäker-Hübner, L.; Christianson, D. W.; Hansen, F. K. Difluoromethyl-1,3,4-Oxadiazoles Are Selective, Mechanism-Based, and Essentially Irreversible Inhibitors of Histone Deacetylase 6. *J. Med. Chem.* **2023**, *66* (19), 13821–13837.